Wetting/dewetting transition of two-phase flows in nano-corrugated channels

Article *in* Journal of Computer-Aided Materials Design · October 2007
DOI: 10.1007/s10820-007-9061-1

CITATIONS
5

5 authors, including:


Luca Biferale
University of Rome Tor Vergata
280 PUBLICATIONS **5,837** CITATIONS
SEE PROFILE


Mauro Sbragaglia
University of Rome Tor Vergata
116 PUBLICATIONS **2,432** CITATIONS
SEE PROFILE


Sauro Succi
INFN - Istituto Nazionale di Fisica Nucleare
551 PUBLICATIONS **17,802** CITATIONS
SEE PROFILE


Federico Toschi
Technische Universiteit Eindhoven
282 PUBLICATIONS **5,758** CITATIONS
SEE PROFILE

J Computer-Aided Mater Des (2007) 14:447–456
DOI 10.1007/s10820-007-9061-1

Wetting/dewetting transition of two-phase flows in nano-corrugated channels

L. Biferale · R. Benzi · M. Sbragaglia · S. Succi · F. Toschi

Received: 24 January 2007 / Accepted: 2 February 2007 / Published online: 2 October 2007

Abstract A lattice version of the Boltzmann kinetic equation for describing multi-phase flows in nano- and micro-corrugated devices is reviewed. To this purpose, the Shan-Chen Lattice Boltzmann model [Phys. Rev. E **47**, 1815 (1993)] for non-ideal fluids is extended to the case of confined geometries with hydrophobic properties on the wall. This extended Shan-Chen method is applied for the simulation of the wetting/dewetting transition in the presence of nanoscopic grooves etched on the boundaries. This approach permits to retain the essential *supra-molecular* details of fluid-solid interactions without surrendering -in fact boosting- the computational efficiency of continuum methods. The method is first validated against the Molecular Dynamics (MD) results of Cottin-Bizonne et al. [Nature Mater. **2**, 237 (2003)] and then applied to more complex geometries, hardly accessible to MD simulations. The resulting analysis confirms that surface roughness and capillary effects can promote a sizeable reduction of the flow drag, with a substantial enhancement of the mass flow rates and slip-lengths, which can reach up to the micrometric range for highly hydrophobic surfaces.

Keywords Microfluidics · Lattice Boltzmann equation · Non ideal fluids

This article is to be regarded part of the first Synergy Between Experiment and Computation in Nanoscale Science (NNIN/C) conference held in Cambridge, Massachusetts, U.S.A., 31 May–3 June 2006 proceedings published in the Journal of Computer-Aided Materials Design, Volume 14, No. 1, 2007.

L. Biferale (✉) · R. Benzi
Dipartimento di Fisica and INFN, Università di Roma "Tor Vergata", Via della Ricerca Scientifica 1, 00133 Rome, Italy
e-mail: biferale@roma2.infn.it

M. Sbragaglia
Department of Applied Physics, University of Twente, P.O. Box 217, 7500 AE Enschede, The Netherlands

S. Succi · F. Toschi
Istituto per le Applicazioni del Calcolo CNR, Viale del Policlinico 137, 00161 Rome, Italy

F. Toschi
INFN, Sezione di Ferrara, via G. Saragat 1, 44100 Ferrara, Italy

The motion of fluids at the micro and nanoscale is controlled by the competition of dissipative effects against pressure drive and eventually capillarity effects. The weakness of inertia in the microworld implies that it is increasingly difficult to push fluids across micro/nanoconfined geometries, due to the increasing surface to volume ratioes. As a result, the dynamics of microflows is crucially affected by the interaction of the fluid with the confining solid boundaries. Information on these interactions is usually conveyed into the formulation of proper boundary conditions for the fluid flow. In particular, slip-flow phenomena (see [21, 23] for recent reviews) have been reported in experiments and in molecular dynamics simulations, depending on the thermodynamical and wetting properties of the boundary (contact angle) and on the surface geometry [2, 12, 14, 15, 24, 30, 33–35]. A basic question arises as to whether the fluid really slips over the surface, or rather the indirect measurements based on pressure/mass flow rate relations or surface force apparatus reflect an apparent slip, arising from surface inhomogeneities or complex additional fluid-interface phenomena.

Indeed, it has been argued that a gas layer at the interface would alter the fluid dynamics in the bulk, leading to a mass-flow rate increase even in the presence of pure no-slip [5, 16, 18, 20, 22, 31]. This hypothesis is supported by the observation of nanobubbles trapped on the surface [32] and by a decreasing apparent slip length as the fluid is degased [17].

The aim of this work is to discuss the complex effects, at the hydrodynamical scales, induced by the surface wetting properties in the presence of complex geometries in micro- and nano-devices. The main result of this work is that the physics of the boundary conditions is quantitatively reproduced by modeling the fluid at a mesoscopic level, i.e. by means of a minimal version of the Boltzmann equation, i.e. the Lattice Boltzmann Equation (LBE) [6, 11, 28]. This result is obtained by performing a quantitative comparison of a "finite-volume" dewetting transition against recent Molecular Dynamics simulations (MD) [13, 14]. Far from being a mere technicality, this result opens the way to numerical investigations at spatial and time scales much larger than those currently available in most MD simulations. Moreover, we extend the MD results by investigating the critical dependency of the mass flow rate on the degree of roughness at constant bulk pressure.

The lattice Boltzmann equation

The simplest LBE reads as follows [7]:

$$f_\alpha(\boldsymbol{x} + \boldsymbol{c}_\alpha \Delta t, t + \Delta t) - f_\alpha(\boldsymbol{x}, t) = -\omega \Delta t [f_\alpha(\boldsymbol{x}, t) - f_\alpha^{(eq)}(\boldsymbol{x}, t)] + F_\alpha \Delta t, \qquad (1)$$

where $f_\alpha(\boldsymbol{x}, t)$ is the probability of finding a particle at site $\boldsymbol{x}$ at time t, moving along one of the α-*th* lattice direction defined by the discrete speed $\boldsymbol{c}_\alpha$ with $\alpha = 1, \ldots, b$ and Δt is the time unit. The left-hand side of (1) stands for molecular free-streaming, whereas the right-hand side represents molecular collisions. These are expressed through a simple relaxation towards local Maxwellian equilibrium $f_\alpha^{(eq)}$ in a time lapse of the order of $\tau \equiv \omega^{-1}$. Finally, the term F_i represents a volumetric body-force, which can be tailored to produce non-trivial macroscopic effects, such as phase-transitions. Non-ideal effects, leading to two-phase flows, are modeled through a self-consistent force term:

$$\boldsymbol{F}(\boldsymbol{x}, t) = -\mathcal{G}_b \sum_\alpha w_\alpha \psi(\boldsymbol{x}, t) \psi(\boldsymbol{x} + \boldsymbol{c}_\alpha \Delta t, t) \boldsymbol{c}_\alpha. \qquad (2)$$

Here, $\psi(\boldsymbol{x})$ is a phenomenological pseudo-potential (generalized density), $\psi(\boldsymbol{x}, t) = \psi[\rho(\boldsymbol{x}, t)]$, first introduced by Shan and Chen [26, 27], W_α are normalization weights and $\mathcal{G}_b$ tunes the molecule-molecule interaction, i.e. it plays the role of the normalized *inverse*

temperature, ϵ/KT, with ϵ the molecular interaction, K The Boltzmann constant and T the system temperature. Here we choose the standard form $\psi = \sqrt{\rho_0}\{1 - \exp(-\rho/\rho_0)\}$, with the reference density $\rho_0 = 1$, in lattice units.

The interaction potential (2) can be regarded as the simplest "mean-field" approximation of the body force induced by soft particle-particle interactions in the collisional term of the Boltzmann Equations [3].

In spite of its simplicity, the Shan-Chen approach provides two crucial ingredients of non-ideal fluid behavior: a non-ideal equation of state and a non-zero liquid-vapor surface tension, σ_{lv}. Both features are encoded in the expression of the non-ideal momentum flux tensor P_{iJ}. In the hydrodynamic limit, the LBE equations (1)–(2) can be shown to evolve according to the Navier-Stokes equations [3], with the following pressure tensor $\overleftrightarrow{P}$:

$$P_{ij} = \left[c_s^2\rho + \frac{1}{2}c_s^2\mathcal{G}_b\psi^2 + \frac{1}{2}c_s^4\mathcal{G}_b\psi\Delta\psi + \frac{\mathcal{G}_b c_s^4}{4}|\nabla\psi|^2\right]\delta_{ij} - \frac{1}{2}c_s^4\mathcal{G}_b\partial_i\psi\partial_j\psi. \tag{3}$$

The relation (3) can be derived by starting from the expression of the i-th component of the interparticle force:

$$F_i(\boldsymbol{x}, t) = -\mathcal{G}_b\psi(\boldsymbol{x})\sum_\alpha w_\alpha\psi(\boldsymbol{x} + \boldsymbol{c}_\alpha\Delta t, t)c_\alpha^i. \tag{4}$$

Assuming a stationary state ($\boldsymbol{F}(\boldsymbol{x}, t) = \boldsymbol{F}(\boldsymbol{x})$) and Taylor expanding for $\Delta t = 1$ up to the third order, we obtain:

$$F_i(\boldsymbol{x}) = -\mathcal{G}_b\psi(\boldsymbol{x})\left[\sum_\alpha w_\alpha c_\alpha^i\psi(\boldsymbol{x}) + \sum_{\alpha,j} w_\alpha c_\alpha^i c_\alpha^j\partial_j\psi(\boldsymbol{x}) + \frac{1}{2}\sum_{\alpha,j,k} w_\alpha c_\alpha^i c_\alpha^j c_\alpha^k\partial_j\partial_k\psi(\boldsymbol{x}) + \frac{1}{6}\sum_{\alpha,j,k,l} w_\alpha c_\alpha^i c_\alpha^j c_\alpha^k c_\alpha^l\partial_j\partial_k\partial_l\psi(\boldsymbol{x})\right].$$

With reference to the standard nine-speed two-dimensional lattice, by choosing the weights w_α as follows: $w_0 = 4/9$ for the rest particle, $w_{1\ldots4} = 1/9$ for speed-one particles (nearest-neighbors), and $w_{5\ldots8} = 1/36$ for speed-$\sqrt{2}$ particles (next-to-nearest neighbors), the following relations are fulfilled:

$$\sum_\alpha w_\alpha c_\alpha^i = 0 \qquad \sum_\alpha w_\alpha c_\alpha^i c_\alpha^j = c_s^2\delta_{ij}$$

$$\sum_\alpha w_\alpha c_\alpha^i c_\alpha^j c_\alpha^k = 0 \qquad \sum_\alpha w_\alpha c_\alpha^i c_\alpha^j c_\alpha^k c_\alpha^l = c_s^4(\delta_{ij}\delta_{kl} + \delta_{ik}\delta_{jl} + \delta_{il}\delta_{jk}).$$

As a result, the i-component of $\boldsymbol{F}$ reads as follows:

$$F_i = -\mathcal{G}_b\psi c_s^2\partial_i\psi - \mathcal{G}_b\psi\frac{1}{2}c_s^4\partial_i\Delta\psi. \tag{5}$$

being Δ the Laplacian operator. The above expression for the interparticle force can be easily translated into an excess pressure with respect to the ideal gas expression ($c_s^2\rho$), using the definition:

$$-\partial_j P_{i,J} + \partial_i(c_s^2\rho) = F_i \tag{6}$$

This leads to a pressure tensor of the form (3).

The equation of state in the bulk is $P = c_s^2\rho + \frac{1}{2}c_s^2\mathcal{G}_b\psi^2$, where we recognize a non-ideal contribution on top of the ideal equation of state $P = \rho c_s^2$ with c_s^2 the sound speed velocity. This equation of state supports a phase-transition at a critical density $\rho_c/\rho_0 = \ln(2)$, whenever the coupling strength exceeds (in magnitude) the critical value $\mathcal{G}_c = -4.0$. As to the velocity field, following [3], we set it to be zero at the boundary by using bounce-back boundary conditions. For the case when slippage properties are imposed a-priori, different boundary conditions should be used [1, 4]. Next, the density field $\rho(\boldsymbol{x})$ is assumed to match a given value $\psi_w = \psi(\rho_w)$, where ρ_w should be regarded as a free-parameter related to the strength of the fluid/solid interactions. In [3], it has been shown that by imposing the condition of mechanical equilibrium, $\partial_j P_{ij} = 0$, of the contact line separating the liquid, vapor and solid phases, one can compute analytically the *contact angle*, $\theta(\mathcal{G}_b, \rho_w)$. The result is:

$$\cos(\theta) = \frac{\int_{sv} |\partial_y\psi|^2 dy - \int_{sl} |\partial_y\psi|^2 dy}{\int_{lv} |\partial_y\psi|^2 dy} \tag{7}$$

where $\int_{sl} |\partial_y\psi|^2 dy$, $\int_{sv} |\partial_y\psi|^2 dy$, $\int_{lv} |\partial_y\psi|^2 dy$ indicate the positive integrals calculated along the solid-liquid, solid-vapor and liquid-vapor interfaces with y the coordinate normal to the interface. Notwithstanding their inherently mesoscopic character, the parameters $\mathcal{G}_b$ and ρ_w carry no less physical content than their atomistic counterparts (relative strength of the attractive to repulsive interactions in MD simulations [8, 25, 30]). It should be emphasized that the contact angle can be computed also within the framework of the free-energy version of the lattice Boltzmann method for non-ideal fluids [10, 29]. Here, however, we prefer to stick to the Shan-Chen pseudo-potential formulation, because of its simplicity. In order to study the wetting/dewetting transition on micro/nano-patterned surfaces (see Fig. 1) we have integrated the LBE equation (1) in a $2D$ Lattice using the nine-speed $2DQ9$ model ($b = 9$), one of the most used $2D$-LBE scheme, due to its superior stability [9, 19]. We have used the two geometries described in Fig. 1. All simulations have been performed at fixed "inverse temperature" $\mathcal{G}_b = -6.0$ i.e. beyond the critical value $\mathcal{G}_b = -4.0$. The relaxation parameter is taken as $\tau = 0.8$ in lattice units. The equation of state delivers the corresponding values of the liquid and vapor density, $\rho_l = 2.65$ and $\rho_g = 0.07$ respectively, while the surface tension is $\sigma_{lv} = 0.105 \pm 0.002$ in lattice units. The value of the lattice spacing in physical units is obtained by matching the physical value of the liquid-vapor surface tension, with the one measured on the lattice, via the dimensional relation: $\sigma_{lv}^{phys} = KT/(\Delta x)^2\sigma_{lv}$. For water/vapor at $T = 540°$, where the density ratio is close to the values of our simulation, we have $\sigma_{lv}^{phys} = 0.022N/m$ which yelds $\Delta x \sim 0.3nm$. This value is comparable with the atomic range of the Lennard-Jones potential used in MD. Molecular dynamics simulations have recently reported that the concerted effects of wetting phenomena and nano-corrugations can lead to a fairly substantial reduction of mechanical drag [13, 14]. Specifically, the authors in [13, 14] consider a nanometric channel flow with a regular sequence of longitudinal or transverse steps (with respect to the mean flow) along the solid wall of the channel, and show that, under suitable thermodynamic and geometric conditions, the presence of the steps triggers the formation of a gas film in the grooves within the obstacles. The liquid can then slide-away over the gas film, thereby experiencing a significantly reduced mechanical drag. Such phenomenon may occur only at a critical pressure drop between liquid

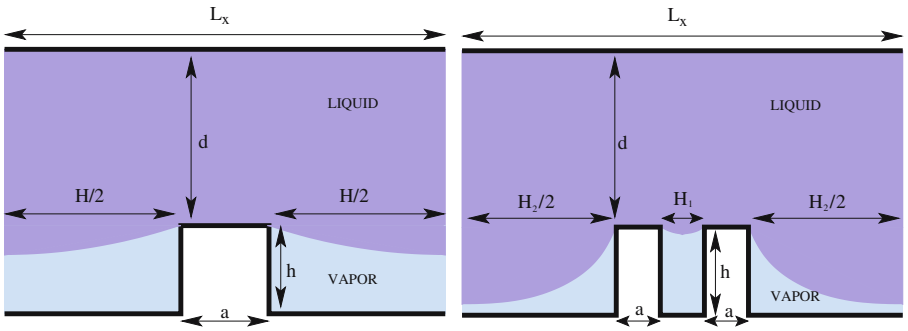

Fig. 1 Left: homogeneous roughness. A groove with depth $h = 33\Delta x$ and width $H = L_x - a$ (with $a = 10\Delta x$) is introduced on the bottom wall and periodic boundary conditions are assumed along x. In this configuration, the presence of vapor pockets inside the groove changes the "effective" boundary conditions felt by the bulk fluid, with a net decrease of drag when a pressure drop is applied. Right: channel with heterogeneous roughness. Two grooves of width $H_1 = 40\Delta x$ and $H_2 = 70\Delta x$ are present. The two grooves are filled separately at different values in the pressure/density diagram. The lattice spacing corresponds to $\Delta x \sim 0.3nm$

and vapor phase, of the order of the capillary pressure, P_{cap}, given by the estimate [13]:

$$P_{cap} = -\frac{2\sigma_{lv}\cos(\theta)}{L_x - a}. \tag{8}$$

In Fig. 2, we validate the LBE by a direct comparison with the MD results published in [13, 14] with the same geometry and with comparable contact angle. In particular, we show the pressure drop between the bulk liquid and vapor phases $\Delta P_{lv} = P_l - P_v$, at changing the distance d (see Fig. 1) at fixed total mass, i.e. at changing the average density. As one can clearly see, the agreement between LBE and MD is quantitative. The plateaux observed for ΔP_{lv} in the range $0.9 < d/L_x < 1.05$ corresponds to the pressure/density values at which the fluid is invading the corrugation, thus forming an interface which does not yet touch the bottom of the groove. This corresponds to the capillary pressure, P_{cap}. By further decreasing d, i.e. by increasing the average density, a change of concavity for $0.8 < d/L_x < 0.9$, is observed. This range corresponds to values such that the interface starts to touch the bottom of the groove, thereby adjusting its pressure/density in such a way as to minimize the free energy in the presence of the new liquid-vapor-solid interface. The agreement of LBE with the capillary pressure (8) is checked in detail in Fig. 3, where we report the change of the pressure diagram with a changing distance d, for three different corrugation values, $L_x - a$. In Fig. 4, we extract the value of $\sigma_{lv}\cos(\theta)$ from the the slope of the observed plateaux $vs\ \Delta x/(L_x - a)$. The value of $\cos(\theta)$ is then obtained by estimating the surface tension, σ_{lv}, through Laplace's law for a droplet in equilibrium with its saturated vapor. The agreement of the contact angle measured in this way, $\theta = 158° \pm 6°$, with the analytical estimate, $\theta = 160°$, obtained by solving (7) for the given density profiles.

The comparison shown in Figs. 2, 3 and 4 demonstrates the first result discussed in this paper, namely that the model introduced in [3] captures the correct interplay between roughness and wetting effects.

Even more complex behavior is observed for heterogeneous nano-corrugations, with the simplest case shown in the right panel of Fig. 1. In this case, one has two characteristic groove sizes, H_1 and H_2, and hence two corresponding critical capillary pressures. The pressure/density diagram for this heterogeneous corrugation is shown in Fig. 5, where the two plateaux

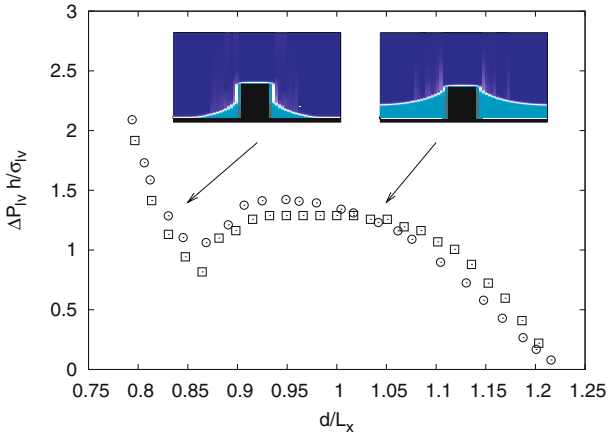

Fig. 2 Validation of our LBE simulation against MD results [13]. The LBE is done with the same aspect-ratios of MD. The dimensionless normalized pressure drop, $\Delta P_{lv} h/\sigma_{lv}$ between the two bulk phases, is shown as a function of the normalized distance d/L_x (see Fig. 1). LBE (□) results have been obtained with a contact angle $\theta = 160°$, which is consistent with the contact angle measured in MD (○) simulation (see Fig. 2 of [13]). The two insets represent the density configuration at the onset of the wetting/dewetting transition (right) and for a wetted configuration (left). The plateaux in the pressure curve defines the capillary pressure, P_{cap}

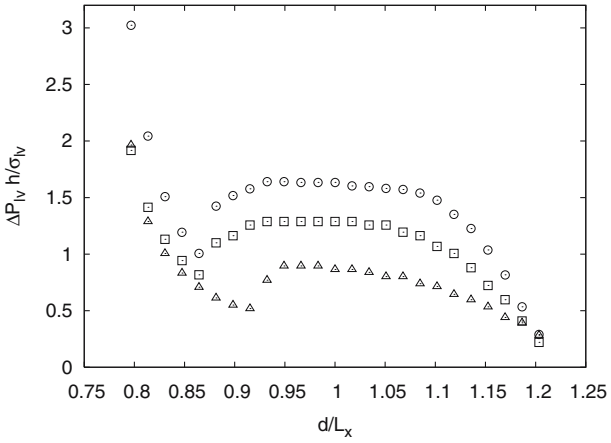

Fig. 3 Pressure variations at changing d for various roughnesses, $L_x = 50\Delta x$ (△), $L_x = 60\Delta x$ (□), $L_x = 80\Delta x$ (○) with $a = 10\Delta x$.

corresponding to the two capillary pressures coexist. This device may be regarded as a "smart" two-state surface, whose wetting properties and mass throughput (under the application of a pressure gradient) may be tuned by changing the bulk pressure.

The dynamical response of the micro-channel is investigated by applying a constant pressure gradient. In Fig. 6, we show the mass-flow rate gain as a function of the degree of roughness, $a/(L_x - a)$, for a fixed groove depth h and at a given normalized pressure drop, $\Delta P_{lv} h/\sigma_{lv} = 0.75$. The main result here is the presence of a transition at a critical roughness, $a/(L_x - a)$, where the mass flow rate starts to increase with respect to the perfect wetting situations reaching as much as 100% gain. The strong dynamical effect of the gas-layer can be appraised in a more detail by inspecting the velocity and momentum profiles along the

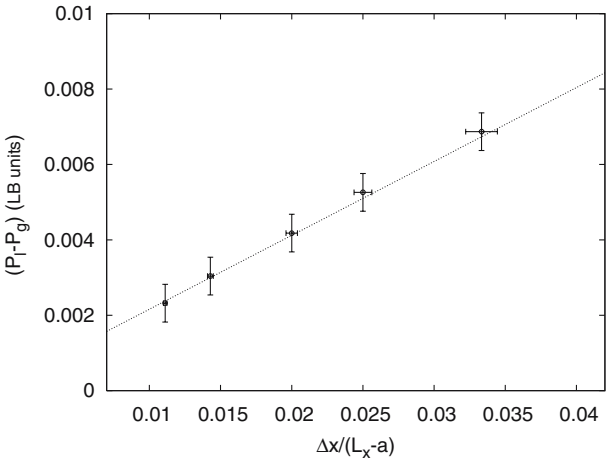

Fig. 4 We show the relation (8). The slope is given by $2\sigma_{lv}\cos(\theta) = -0.196 \pm 0.006$ (LB units). With our surface tension $\sigma_{lv} = 0.105 \pm 0.002$ (LB units), this implies a best estimate of $\theta = 158° \pm 6°$

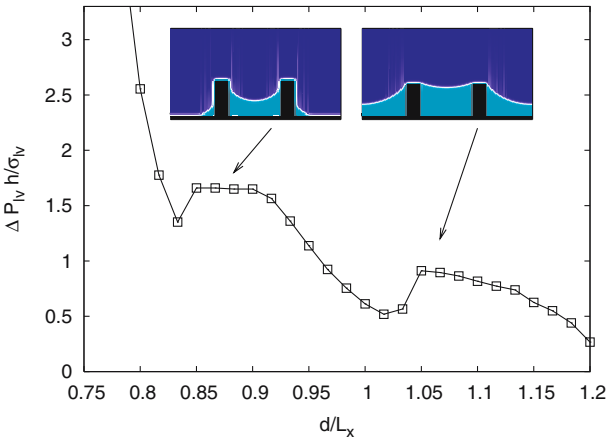

Fig. 5 Pressure variations at changing d, with fixed total mass for the case of heterogeneous roughness (see right panel of Fig. 1). The two plateaux correspond to the case in which the liquid is starting to invade the widest groove (right) and when it is invading also the thinnest (left)

vertical direction, without the vapor layer (fully-wetted configuration) and with a thin vapor layer starting to accumulate close to the bottom of the groove. This is shown in Fig. 7, where the *local* slip length is also reported by extrapolation of the bulk profile inside the wall. As soon as a vapor layer is formed, the *local* slip-length ramps-up, reaching values of the order of the channel height $45\Delta x \sim 15nm$. Even larger values can be measured close to the dewetting transition, where a well-developed vapor layer is formed inside the groove (the so-called *super-hydrophobic regime*).

Summarizing, we have shown that an extension of lattice Boltzmann equation for non-ideal fluids, can *quantitatively* account for the concerted effects of wetting phenomena and geometrical irregularities. In particular, the presence of nano/micro-irregularities in the flow geometries is shown to lead to sizeable effects with respect to the *infinite volume* liquid-gas

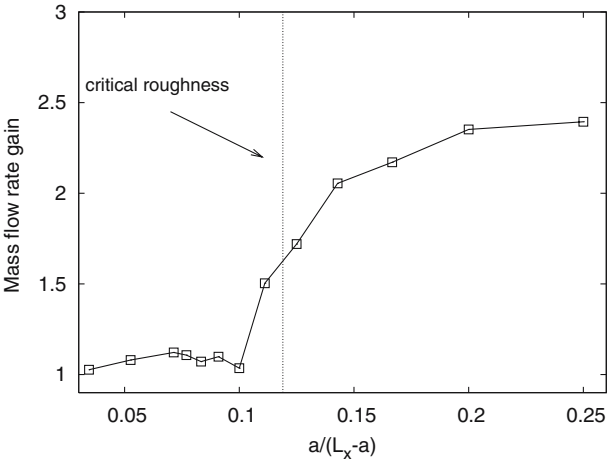

Fig. 6 Mass flow rate normalized to fully wetted case *vs* the effective roughness $a/(L_x - a)$. The bulk pressure is fixed to be $\Delta P_{lv} = 0.75\sigma_{lv}/h$. A critical roughness (vertical line) is given by the estimate of the capillary pressure, $0.75\frac{a}{2h\cos(\theta)} = 0.119$ for $a = 10\Delta x$, $h = 33\Delta x$, $\theta = 158^\circ$

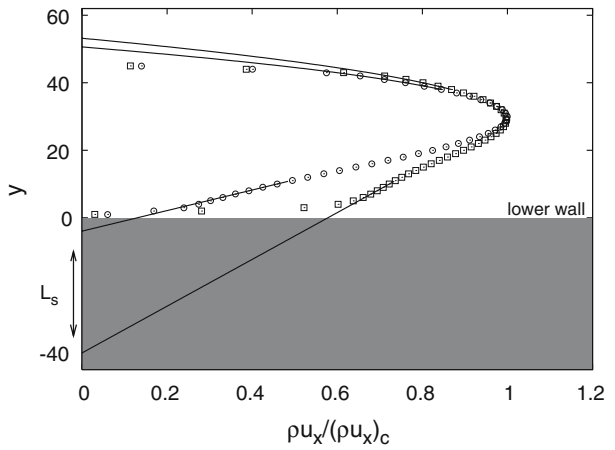

Fig. 7 Vertical momentum profile for a wetted (○), and almost dewetted configuration (□). The geometry is fixed to the one of the left panel of Fig. 1 with parameters $h = 14\Delta x$, $a = 14\Delta x$, $L_y = 45\Delta x$, $L_x = 90\Delta x$. Both momentum profiles are shown for $x/L_x = 0.1$ and normalized with their center channel values. The straight lines correspond to extrapolations of the profiles inside the boundaries, i.e. the standard way to define a slip-length

transitions, and to a consequent significant reduction of mechanical drag on the flowing fluid. The present results indicate that drag-reduction via geometry-induced wetting transitions is a non-specific phenomenon, which depends on the contact angle, but not by the details of many-body molecular interactions behind it. The mesoscopic LBE approach presented here offers the opportunity to efficiently simulate complex micro/nanofluidic phenomena at scales of direct experimental relevance, which are totally unpractical for atomistic simulations. This may open the way to the systematic optimization of microfluidic devices via computer simulation. Useful discussions with J.-L. Barrat, X. Shan and S. Troian are kindly acknowledged.

References

1. Ansumali, S., Karlin, I.V.: Kinetic boundary conditions in the lattice Boltzmann method. Phys. Rev. E **66**(2), 026311 (2002)
2. Baudry, J., Charlaix, E., Tonck, A., Mazuyer, D.: Experimental evidence for a large slip effect at a nonwetting fluid-solid interface. Langmuir **17**(17), 5232–5236 (2001)
3. Benzi, R., Biferale, L., Sbragaglia, M., Succi, S., Toschi, F.: Mesoscopic modeling of a two-phase flow in the presence of boundaries: the contact angle. Phys. Rev. E **74**(2), 021509 (2006)
4. Benzi, R., Biferale, L., Sbragaglia, M., Succi, S., Toschi, F.: Mesoscopic modelling of heterogeneous boundary conditions for microchannel flows. J. Fluid Mech. **548**, 257–280 (2006)
5. Benzi, R., Biferale, L., Sbragaglia, M., Succi, S., Toschi, F.: Mesoscopic two-phase model for describing apparent slip in micro-channel flows. Europhys. Lett. **74**(4), 651–657 (2006)
6. Benzi, R., Succi, S., Vergassola, M.: The lattice boltzmann-equation—theory and applications. Phys. Report **222**(3), 145–197 (1992)
7. Bhatnagar, P.L., Gross, E.P., Krook, M.: A model for collision processes in gases. 1. Small amplitude processes in charged and neutral one-component systems. Phys. Rev. **94**(3), 511–525 (1954)
8. Bocquet, L., Barrat, J.L.: Hydrodynamic boundary-conditions and correlation-functions of confined fluids. Phys. Rev. Lett. **70**(18), 2726–2729 (1993)
9. Boghosian, B.M., Yepez, J., Coveney, P.V., Wager, A.: Entropic lattice boltzmann methods. Proc. R. Soc. London A **457**(2007), 717–766 (2001)
10. Briant, A.J., Papatzacos, P., Yeomans, J.M.: Lattice boltzmann simulations of contact line motion in a liquid-gas system. Phil. Trans. R. Soc. Lond. A **360**(1792), 485–495 (2002)
11. Chen, S., Doolen, G.D.: Lattice boltzmann method for fluid flows. Annu. Rev. Fluid Mech. **30**, 329–364 (1998)
12. Cheng, J.T., Giordano, N.: Fluid flow through nanometer-scale channels. Phys. Rev. E **65**(3), 031206 (2002)
13. Cottin-Bizonne, C., Barentin, C., Charlaix, E., Bocquet, L., Barrat, J.L.: Dynamics of simple liquids at heterogeneous surfaces: Molecular-dynamics simulations and hydrodynamic description. Eur. Phys. J. E **15**(4), 427–438 (2004)
14. Cottin-Bizonne, C., Barrat, J.L., Bocquet, L., Charlaix, E.: Low-friction flows of liquid at nanopatterned interfaces. Nat. Mater. **2**(4), 237–240 (2003)
15. Cottin-Bizonne, C., Jurine, S., Baudry, J., Crassous, J., Restagno, F., Charlaix, E.: Nanorheology: an investigation of the boundary condition at hydrophobic and hydrophilic interfaces. Eur. Phys. J. E **9**(1), 47–53 (2002)
16. de Gennes, P.G.: On fluid/wall slippage. Langmuir **18**(9), 3413–3414 (2002)
17. Granick, S., Zhu, Y.X., Lee, H.: Slippery questions about complex fluids flowing past solids. Nat. Mater. **2**(4), 221–227 (2003)
18. Harting, J., Kunert, C., Herrmann, H.J.: Lattice boltzmann simulations of apparent slip in hydrophobic microchannels. Europhys. Lett. **75**(2), 328–334 (2006)
19. Karlin, I.V., Ferrante, A., Ottinger, H.C.: Perfect entropy functions of the lattice boltzmann method. Europhys. Lett. **47**(2), 182–188 (1999)
20. Lauga, E., Brenner, M.P.: Dynamic mechanisms for apparent slip on hydrophobic surfaces. Phys. Rev. E **70**(2), 026311 (2004)
21. Lauga, E., Brenner, M.P., Stone, H.A.: Microfluidics: the no-slip boundary condition. Handbook of Experimental Fluid Dynamics, pp 1240. Springer (2007)
22. Li, B.M., Kwok, D.Y.: Discrete boltzmann equation for microfluidics. Phys. Rev. Lett. **90**(12), 124502 (2003)
23. Neto, C., Evans, D.R., Bonaccurso, E., Butt, H.J., Craig, V.S.J.: Boundary slip in newtonian liquids: a review of experimental studies. Rep. Prog. Phys. **68**(12), 2859–2897 (2005)
24. Ou, J., Rothstein, J.P.: Direct velocity measurements of the flow past drag-reducing ultrahydrophobic surfaces. Phys. Fluids **17**(10), 103606 (2005)
25. Priezjev, N.V., Darhuber, A.A., Troian, S.M.: Slip behavior in liquid films on surfaces of patterned wettability: comparison between continuum and molecular dynamics simulations. Phys. Rev. E **71**(4), 041608 (2005)
26. Shan, X.W., Chen, H.D.: Lattice boltzmann model for simulating flows with multiple phases and components. Phys. Rev. E **47**(3), 1815–1819 (1993)
27. Shan, X.W., Chen, H.D.: Simulation of nonideal gases and liquid-gas phase-transitions by the lattice boltzmann-equation. Phys. Rev. E **49**(4), 2941–2948 (1994)
28. Succi, S.: The Lattice Boltzmann Equation. Oxford Science (2001)

29. Swift, M.R., Osborn, W.R., Yeomans, J.M.: Lattice Boltzmann simulation of nonideal fluids. Phys. Rev. Lett. **75**(5), 830–833 (1995)
30. Thompson, P.A., Troian, S.M.: A general boundary condition for liquid flow at solid surfaces. Nature **389**(6649), 360–362 (1997)
31. Tretheway, D.C., Meinhart, C.D.: Apparent fluid slip at hydrophobic microchannel walls. Phys. Fluids **14**(3), L9–L12 (2002)
32. Tyrrell, J.W.G., Attard, P.: Images of nanobubbles on hydrophobic surfaces and their interactions. Phys. Rev. Lett. **8717**(17), 176104 (2001)
33. Watanabe, K., Udagawa, Y., Udagawa, H.: Drag reduction of Newtonian fluid in a circular pipe with a highly water-repellent wall. J. Fluid Mech. **381**, 225–238 (1999)
34. Zhu, Y.X., Granick, S.: Rate-dependent slip of newtonian liquid at smooth surfaces. Phys. Rev. Lett. **8709**(9), art. no.–096105 (2001)
35. Zhu, Y.X., Granick, S.: Limits of the hydrodynamic no-slip boundary condition. Phys. Rev. Lett. **88**(10), 106102 (2002)